Supporting Information for:

Dopant Segregation in Polycrystalline Monolayer Graphene

Liuyan Zhao[*,‖], Rui He[*,ŧ,‖], Amir Zabet-Khosousi[‡], Keun Soo Kim[*,§], Theanne Schiros[¶], Michael Roth[ŧ,⊥], Philip Kim[*,#], George W. Flynn[‡], Aron Pinczuk[*,#], Abhay N. Pasupathy[*,□]

[*] Department of Physics, Columbia University, New York, New York, 10027, United States

[ŧ] Department of Physics, University of Northern Iowa, Cedar Falls, Iowa, 50614, United States

[‡] Department of Chemistry, Columbia University, New York, New York, 10027, United States

[§] Department of Physics and Graphene Research Institute, Sejong University, Seoul 143-747, Korea

[¶] Energy Frontier Research Center, Columbia University, New York, New York, 10027, United States

[⊥] Department of Physics and Geology, Northern Kentucky University, Highland Heights, KY 41099, United States

[#] Department of Applied Physics & Applied Mathematics, Columbia University, New York, New York, 10027, United States

[‖] *equal contribution*

□ *corresponding author*

Contents:

S1. Preparation of graphene films by chemical vapor deposition

To investigate the effect of the growth conditions on the results we obtain, we performed growth experiments with two types of precursor gases. The first type is a mixture of H_2, CH_4 and NH_3[1] , and the second is pyridine vapor, a single source for both N and C[2]. Here, we denote the samples prepared by the first recipe as NG_*X* m, where NG stands for N-doped graphene and *X* m for a growth time of *X* minutes, and the sample grown with the second method by NG_Pyridine. Samples were characterized by micro-Raman spectroscopy after transferring onto SiO_2/Si substrates (see section S2 below), using a Renishaw inVia Raman Microscope with 532nm laser excitation and a 100x objective lens which focused the laser to a spot size of ~0.5 μm. Raman spectra and Raman maps were obtained at a room temperature with a scanning step size of 0.4 μm.

(a) Precursors of H_2, CH_4 and NH_3

The copper foil substrate was precleaned with a flow of 10 sccm of H_2 at a pressure of 0.055 torr and a temperature of 1000 ^oC for 10 mins. Doped graphene films were then synthesized using a mixture of H_2 (10 sccm), CH_4 (170 sccm) and NH_3 (0.10 torr partial pressure) at a total pressure of 1.9 torr and a temperature of 1000 ^oC for growths of 5 mins (NG_5m), 8 mins (NG_8m), 10 mins (NG_10m), 14 mins (NG_14m) and 18 mins (NG_18m).

(b) Precursor of Pyridine

The copper foil substrate was first cleaned in ultra-high-vacuum (UHV) by Ar^+ ion bombardment and post-annealing cycles to obtain a fresh copper surface. Doped graphene films were then grown using Pyridine at a pressure of 1 mtorr and a temperature of 950 ^oC for 30 mins, denoted as NG_Pyridine.

S2. Transfer of doped graphene films to SiO_2/Si substrates

N-doped graphene films were transferred onto SiO_2/Si substrates for subsequent micro-Raman measurements. The graphene films on copper foil were first coated with a 200 nm thick layer of PMMA. The underlying copper substrate was then etched away by $FeCl_3$ (20 wt%) solution. The PMMA/graphene membrane then floated on the surface of $FeCl_3$ solution and was scooped using a SiO_2/Si substrate. The graphene/PMMA films were rinsed several times in deionized water before they are dried in air. Finally, the PMMA layer is removed by acetone solution.

S3. X-ray Photoelectron Spectroscopy (XPS)

XPS provides quantitative information on the percentage atomic concentration of various elements in the graphene film. Shown in figure S1 is the N1s XPS for a pristine graphene (PG) film and a nitrogen-doped (NG_10m) film, both in the as-grown condition[3]. The weak, broad peak at ~400 eV binding energy (BE) in the NG_10m film can be assigned to graphitic nitrogen dopants in agreement with studies of modified carbon films. Using tabulated photoelectron cross-sections of nitrogen and carbon (see published work[3] for typical C1s spectra), a total nitrogen concentration of ~0.4% is obtained for the NG_10m graphene.

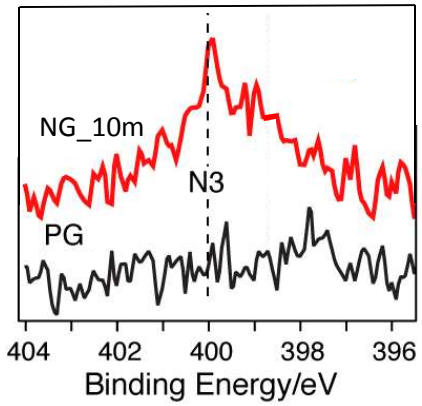

Fig. S1 XPS spectra of pristine (PG) and nitrogen doped (NG_10m) graphene. The position of the peak corresponds to graphitic (N3) doping of nitrogen, and comparison of the peak intensity with the C1s spectrum (not shown) yields a doping level of 0.4% N/C.

S4. Scanning NEXAFS measurements

We utilize Carbon and Nitrogen core-level near edge x-ray absorption spectroscopy (NEXAFS) in partial electron yield (PEY) mode to access direct information on the dopant bond type, orientation and concentration in the doped graphene films. Recently, it has become possible to perform scanning NEXAFS measurements across a sample to probe the dopant nature over large areas. We have performed such measurements using the inaugural Large Area Rapid Imaging Analytical Tool (LARIAT) MKI, at Brookhaven National Laboratory National Synchrotron Light Source (NSLS) beam line U7A. The LARIAT MKI, incorporates: a full field soft x-ray source; electrostatic and magnetostatic electron optical elements to discriminate energy and depth of the secondary electron distribution and; a highly parallel electron detector. The rapid parallel process produces a series of two-dimensional images as the incident soft X-ray energy is scanned above a given absorption edge; here the carbon and nitrogen K-edges, respectively. Synthesis of the image stack produces spatially resolved NEXAFS data that contains direct information about the local electronic and geometric structure, including bond type, concentration and orientation. The electrons are transmitted through the electron optics with nearly 100% efficiency to the imaging detector allowing for high throughput scanning (~725 images/hour) and providing a lateral resolution better than 100-microns over a 23 mm^2 field of view as well as *sub-monolayer molecular sensitivity*. These features make this unique spectrometer particularly well suited to study the local bond environment of N dopants in single layer graphene.

The LARIAT detector uses magnetic projection to image electrons; electrons follow magnetic field lines to form a parallel imaging system. X-ray stimulated electrons emitted from the surface are collected in parallel from all emission angles (when no energy filtering is applied) across the entire field of view and over a high depth of field. Deflection optics scan the synchrotron source beam rapidly across an area up to 20X20 mm^2 while the energy is tuned across an absorption edge. Photon energy incident on the sample at resonance with an absorption edge region stimulates a highly sensitive bond dependent yield of electrons across the surface, the essence of the NEXAFS process. With the sample immersed in a high axial magnetic field coupled with a parallel magnetic field at the imaging detector, the LARIAT detects all emitted secondary electrons in parallel while preserving the spatial relationship originating from the sample. Polarization-dependent NEXAFS data were obtained by changing the angle between the incoming x-ray beam from near-parallel (20°) and near-normal (80°) incidence. A linear background was subtracted as determined from a region before the absorption edge (385-393 eV) and spectra were normalized by area in the post-continuum region between 430 and 440 eV in the case of nitrogen. Carbon and Nitrogen K-edge NEXAFS collection was performed in PEY mode with a grid bias of -200 V and -250 eV, respectively, to optimize the surface sensitivity of the measurement and thereby the signal from the graphene film.

We use the graphene-coated copper foils from the same batch and same process conditions as used for the Raman and STM measurements. Our samples are introduced into the vacuum chamber and annealed for 12 hours at 300^o C before measurement. We use N 1s and C 1s NEXAFS spectra to identify N-dopant bond type and orientation and the scanning capability of the LARIAT detector to identify the spatial distribution of N-dopants, obtained by scanning the sample at a single x-ray energy corresponding to energy of specific N-C XAS π^* resonance. The N 1s NEXAFS spectra typical of these samples, in Fig. S2A, shows sharp peaks with strong angular dependence at ~400.8 and 408 eV,

corresponding to 1*s* to π* and σ* transitions, respectively, of a nitrogen dopant atom substitutionally sp^2-bonded bonded to three carbon neighbors[3] . The angular dependence of the nitrogen data follows that of the carbon NEXAFS, indicating that the features are due to planar N=C bonds in the graphene sample. Fig. S2B shows the typical distribution of graphitic N-dopants in these samples, obtained by scanning the sample at a fixed x-ray energy of 400.8 eV (the energy of the N=C π* resonance).[i] In this figure, the color scale represents the intensity of the π* resonance measured at an incident angle of 30°. While the spatial resolution is limited to about 50 μm, the figure clearly shows the presence of graphitic nitrogen over large areas of the sample. We note that variations in intensity in this figure are primarily caused by roughness of the copper foils on which the growth is performed.

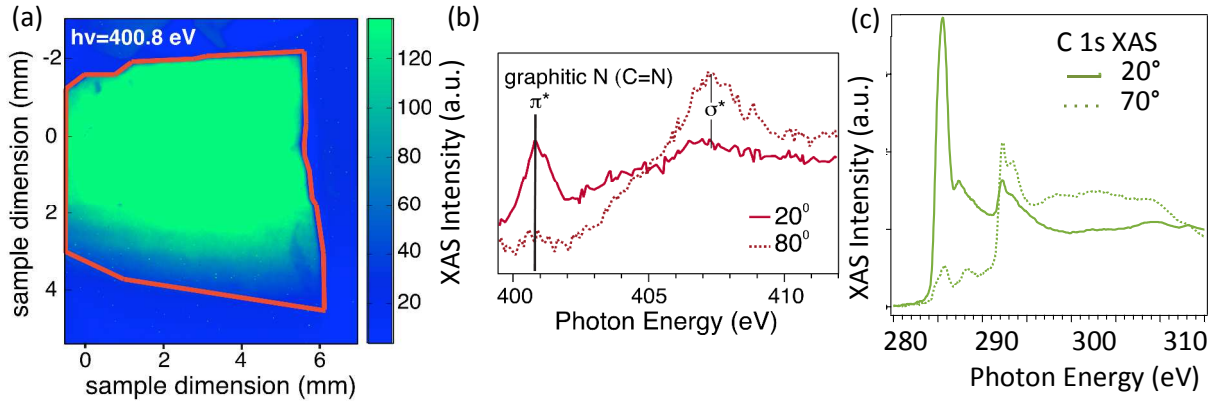

Fig. S2: Nitrogen bond type and distribution observed in N-with micro-XAS of N-doped graphene monolayers on Cu foil. (a) Micro-XAS image, measured at an incident angle of 30° and fixed x-ray energy of 400.8 eV, corresponding to the N=C π * resonance, showing the distribution of graphitic N-dopants over large areas of the sample. (b) N 1s and (c) C 1s XAS spectra measured for polarizations corresponding to the electric field vector of the incoming x-ray beam roughly out-of-plane and in-plane with regard to the graphene surface. The strong polarization dependence reflects planar sp^2 bonds for both N and C.

S5. Atomic resolution STM topography for substitutional N dopants in graphene

Fig. S3 (a) shows a STM topography of as-grown N-doped graphene film on Cu foil over a $50 \times 50\mathrm{nm}^2$ area. Despite the background roughness from the Cu foil substrate, bright features are observed over this sample, which are not seen in pristine graphene films. This fact indicates that these bright features are associated with N dopants. Moreover, same bright features are observed in as grown N-doped graphene film on Cu(111) single crystal (Fig. S3 (b)) A high resolution STM topography over one of this bright features is displayed in Fig. S3 (c). As seen, the bright feature shows up as a triangle pattern formed by three bright spots. The perfect honeycomb lattice is recovered within a few nanometers from the bright feature. The overlaid honeycomb lattice mesh indicates that the center (a blue dot) of the triangle is a C site where a N dopant replaces the C atom, and the three bright spots (three green dots) are at the three first neighboring C sites from the N dopants. The apparent height of the triangle feature

is ~0.7Å (shown in Fig. S3 (d)), further confirming that the N atom stays in the plane of graphene lattice. Given the geometry and apparent height of the N-associated features, we conclude that the N atom replaces a single C atom and forms in-plane sp^2 bonds with the three nearest C atoms, which is the definition of a substitutional N dopant. More detailed descriptions are discussed in our previous work, Ref. 30 in main text.

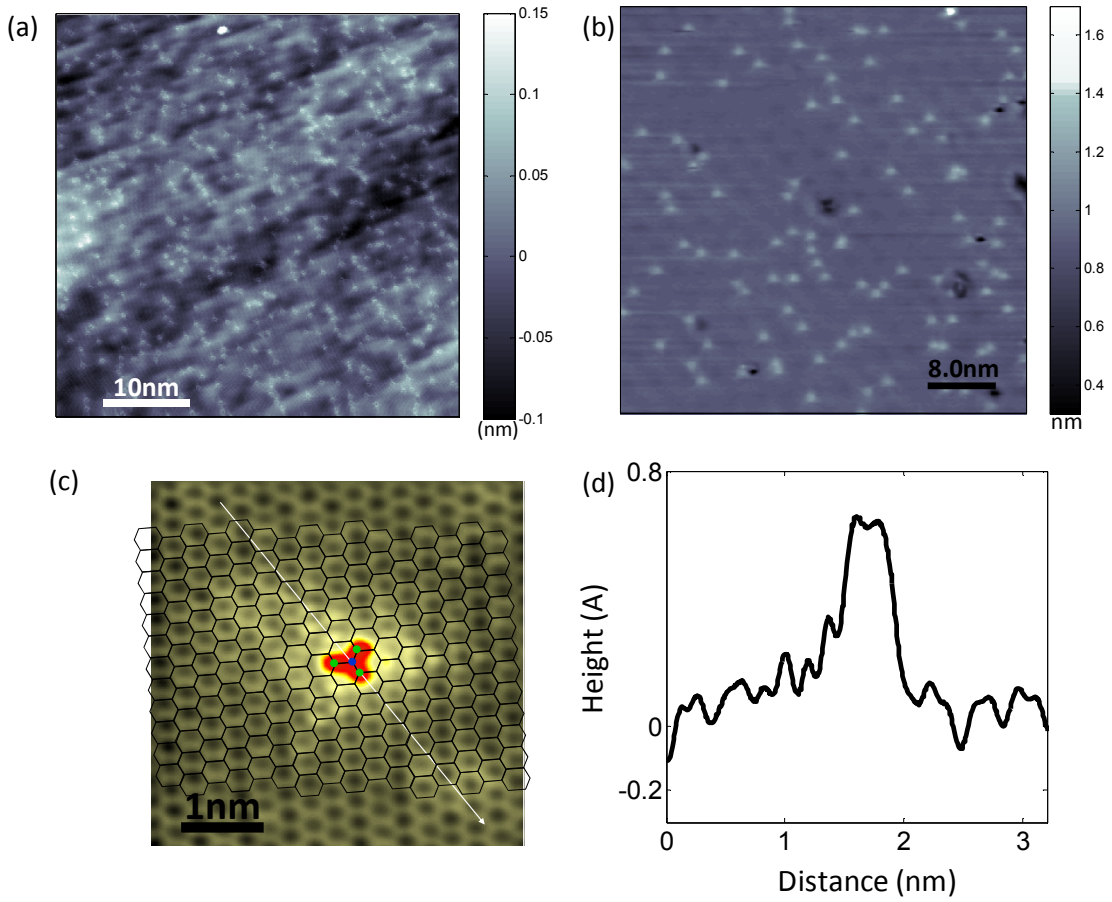

Fig. S3 (a) A $50 \times 50\mathrm{nm}^2$ STM topography of as-grown N-doped graphene film on Cu foil substrate; (b) A $40 \times 40\mathrm{nm}^2$STM topography of as-grown N-doped graphene film on Cu(111) single crystal substrate; (c) An atomic resolution STM topography over a single graphitic N dopant in graphene lattice, with the perfect honeycomb lattice overlaid on top. The center blue dot highlights the N dopant site, and the three green dots are for the first neighboring C sites from N the dopant; (d) A line profile taken along the arrow in (c).

S6. Effect of N dopant on graphene structure in DFT

In order to study the structural effects of defects in graphene, we perform first-principles calculations of the relaxed structure using density functional theory (DFT). DFT calculations are performed within the local density approximation (LDA) as implemented in the Quantum Espresso (QE) package[4] for (a) a single nitrogen dopant in graphene and (b) for a single vacancy in graphene. Structures are relaxed for a

sequence of supercell sizes (5x5, 7x7 and 9x9) containing a single defect in the center, and the consistency of results is checked as a function of cell size. The results of these calculations are shown in figure S4. It is seen that the structural effect of the N dopant in the graphene lattice is extremely small. The nearest neighbor bonds are compressed by merely 0.6%, and some of the further neighbors show expanded bond lengths of up to 0.5%. In contrast, the vacancy shows a 3% compression of bond lengths in its immediate vicinity, and bond length extensions of up to 2% at larger distances. This shows that the nitrogen dopant causes a minimal structural distortion to the graphene lattice, and as a consequence the G peak shift of the Raman spectrum of n-doped graphene is primarily from charge doping rather than strain.

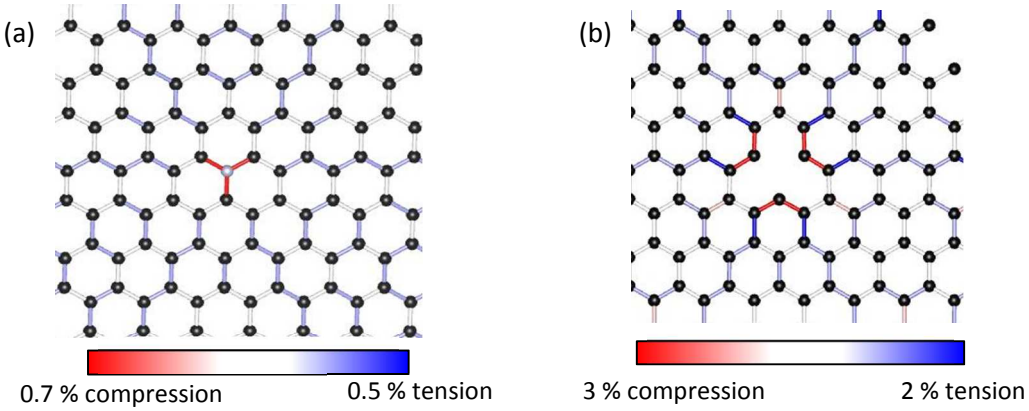

Fig. S4 First principles DFT calculations of the structure of (a) a single N dopant and (b) a vacancy in graphene. The N dopant stays in the plane of the graphene and produces a small distortion of the lattice in its vicinity, while the vacancy produces a distortion that is approximately four times larger in magnitude.

S7. Calculations of the widths of the N-dopant-depleted boundaries

The width of the N-dopant-depleted boundaries was calculated in two steps under the assumption that $width = area/circumference$. The first step is to determine the circumference of the grain boundaries. We use the example of Fig. 2e (see Fig. S5(a)). The cartoon outlines the grain boundaries, from which the total length of the boundaries could be calculated, 247 μm. The second step is to find the area of the N-dopant-depleted region. From the descriptions in the main text, the N-depleted regions have low D/2D ratio and low 2D width as revealed in micro-Raman maps in the paper. Therefore, we select the areas that satisfy: (1) the lowest 5% of the D/2D range; (2) 2D smaller than 45 cm^{-1} in order to exclude bilayer cases. In the case of Fig. 2e, we select the areas which have D/2D<5%×(2.0-0.1)+0.1=0.195 and 2D width < 45 cm^{-1}. These selected areas are shown in Fig. S5(b) with red color, from which we can calculate the corresponding area, 186 μm^2. Simply taking the ratio of area to circumference gives an average width of 0.75 μm.

Using the similar method, we get the average width for each growth (NG_5m, NG_8m, NG_10m, NG_14m and NG_Pyridine) and plot them in Fig. S5(c).

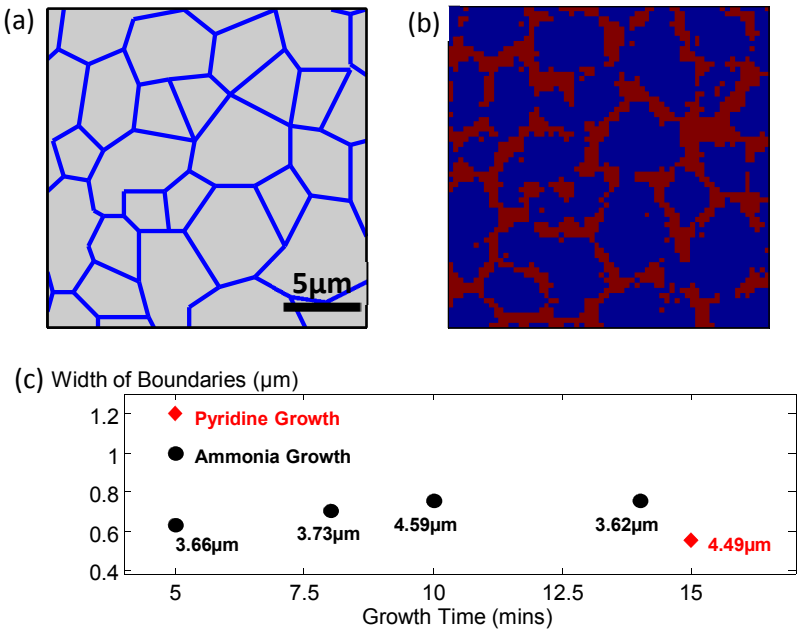

Fig. S5(a) Cartoon of the outline of grain boundaries in Fig. 2e. The circumference calculated from this outline is 247 µm. (b) Selection of areas (red) with low D/2D ratio (N-depleted region) in Fig. 2e. The area of the selected area is 186 μm^2. (c) Widths of the N depleted region for multiple N-doped graphene films (NG_5m, NG_8m, NG_10m, NG_15m and NG_Pyridine). The numberlabeled next to each point is the average grain size of each film with different growth time.

S8. Original large scale STM image on as-grown N-doped graphene on copper foil

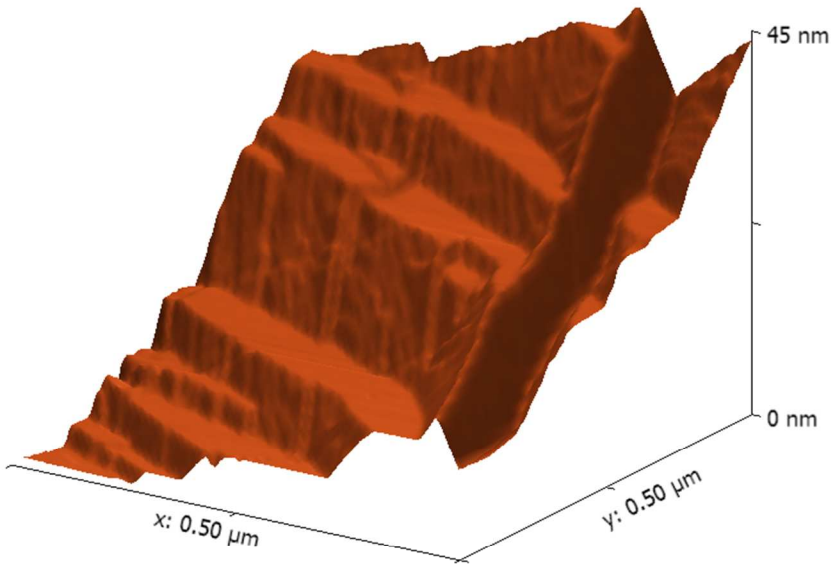

Fig. S6 Three-dimensional topography of Cu foil surface (Original image for Fig. 4a).

S9. Electronic Transport measurements on N-doped graphene films

To understand the effect of chemical doping on the electronic transport properties of N-doped graphene films, four-probe resistivity measurements were carried out on films that were removed from the copper substrate and transferred onto insulating hexagonal boron nitride (hBN) substrates. hBN was chosen as a substrate since it is known from previous measurements that it does not induce significant carriers into graphene films[5]. The transfer process begins by mechanically exfoliating hBN flakes using scotch tape onto Si wafers that are coated with 300 nm of SiO_2. A suitable flake with a thickness ~ 10-15 nm is chosen after performing atomic force microscopy measurements to check for flatness. The substrates are then annealed at 350° C in 5% H_2 and 95% Ar at atmospheric pressure for 9 hours to remove scotch tape residue. Monolayer N-doped graphene (NG10) is then grown on copper substrates as described earlier. The graphene coated copper substrate is placed on a substrate of polydimethylsiloxane (PDMS) and immersed in ammonium persulfate to etch away the copper, leaving behind the NG10 film on the PDMS substrate. The film is rinsed in deionized water to remove contamination and dried in air. Raman spectroscopy is then performed as described earlier to determine the grain boundaries of the NG10 film, and an area of the film is chosen where the doping is uniform. The film is then transferred onto the hBN substrate at 75° C and the PDMS substrate is removed leaving behind the NG10 film on BN. The film is then cleaned in chloroform overnight. Finally, electron-beam lithography is used to define the NG10 channel as well as to define the electrical contacts. Electrical contact is made using 1 nm Cr followed by 15 nm of Pd followed by 40 nm of Au, followed by liftoff to produce the final device as shown in Fig. S7a. The transport device is finally annealed at 350° C in pure Ar at atmospheric pressure for 9 hours to remove residual contamination. Raman spectroscopy is performed again to make sure that the graphene film quality has not changed due to the processing steps performed.

The resistance of a typical NG10 device at room temperature as a function of gate voltage applied to the silicon wafer is shown in Fig. S7b. It is clearly seen that the Dirac point of the film lies below the Fermi level. This behavior has been consistently observed in multiple N-doped graphene films. Control experiments on pristine graphene produced by the same method show no carrier doping, thus showing that the carrier doping in the NG10 film is a result of the N dopants present in the film. From the capacitance of the gate electrode, we can estimate that the carrier doping of the NG10 film is ~ 3×10^{12} electrons/cm^2, showing clearly that N dopants do indeed contribute mobile carriers into graphene.

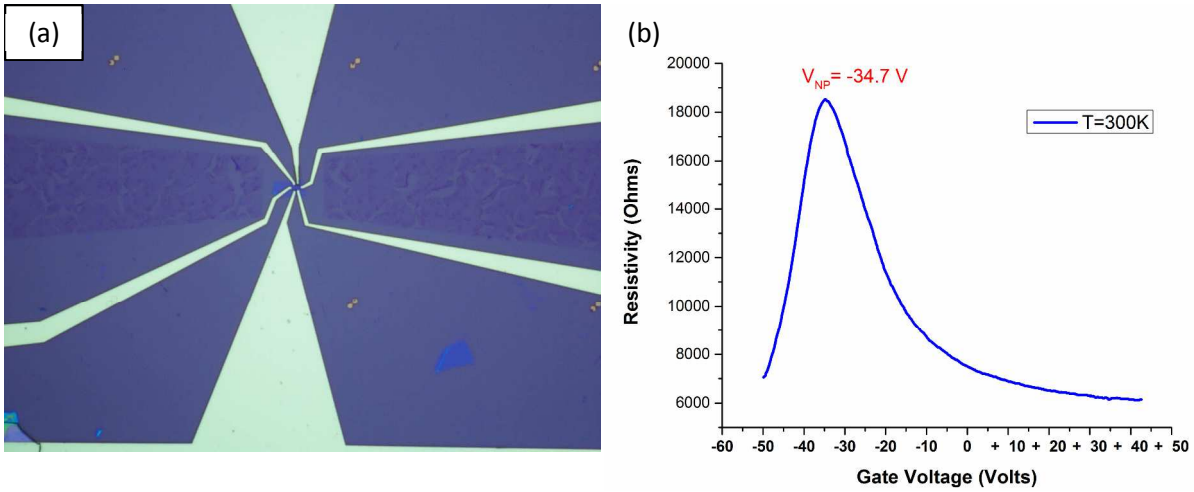

Fig. S7 (a) Optical image of an NG10 device on a hBN/SiO_2/Si substrate with 2 micron channel length shown with six electrical contacts. (b) Resistance versus back gate voltage for this device measured at room temperature. The Dirac point is at -34.7 Volts which corresponds to a carrier concentration at the Fermi level of ~ 3 X 10^{12} electrons/cm^2.

S10. Monte Carlo Simulations

To gain understanding on our experimental results, we performed Monte Carlo simulations on Nitrogen dopant distribution near edges of graphene flakes for multiple sizes and near a single structure grain boundary inside the graphene flake.

(a) Boundary conditions in the simulations

To simulate the experimental conditions at the complex growth temperature of 1000^0C, we tested various boundary conditions. These include (i) a single static graphene flake with free boundary conditions in the horizontal (x,y) plane as well as in the vertical (z) direction; (ii) a single breathable graphene flake with clamped boundary conditions in the (x,y) plane and free in the vertical (z) direction; and finally (iii) a finite-sized graphene sheet with the same boundary conditions as in (i) but with an internal grain boundary introduced. The purpose of free standing boundary conditions in (i) and (ii) is to offer a discontinuity in coordination, reflecting what would be seen at a grain boundary, but the last case (iii) is clearly more realistic topologically than either of the former two, and there the behavior of the dopants at the grain boundary internal to the edges are of interest.

(b) Interactions in the simulations

There are two types of atomicstic interactions in the simulation: bonded and non-bonded ones. The first non-bonded interaction between two atoms is represented as a lattice sum of coulomb interactions. Such an interaction is present to take into account differing electro-negativities between dopants and host atoms. Although the simulation results are quite insensitive to the strength of the Coulomb interaction, it could have an effect at higher dopant concentrations or

at lower temperatures. The second non-bonded interaction is expressed through the Lennard-Jones potential, which expresses the effects of the fluctuating dipoles as well as electron repulsion between non-bonded species. The bonded interaction is the extended reactive empirical bond order (REBO) Brenner-Tersoff potential[6]. The REBO potential takes coordination into account and has been extensively used in simulations of Fullerenes, graphite, graphene and other carbon nanostructures. For the first two cases mentioned earlier, we run simulations with lattice sizes of 2.41×1.35 nm^2, 4.97×2.83nm^2, 15.2×8.73nm^2 and 25.4×14.6nm^2. Such initial and boundary conditions would more accurately account for natural relaxation expressed by the system under the constraint of grain boundaries, and more effectively simulate the effect of strain caused by the boundaries. The grain boundaries reported experimentally and theoretically[7] in graphene involve networks of 5 and 7 membered carbon rings and the structure chosen in our calculations is based on a 19.2×5.9nm^2 graphene flake where the grain boundary is straight.

References:

1. Wei, D.; Liu, Y.; Wang, Y.; Zhang, H.; Huang, L.; Yu, G. *Nano Letters* **2009,** 9, (5), 1752-1758.
2. Jin, Z.; Yao, J.; Kittrell, C.; Tour, J. M. *ACS Nano* **2011,** 5, (5), 4112-4117.
3. Schiros, T.; Nordlund, D.; Pálová, L.; Prezzi, D.; Zhao, L.; Kim, K. S.; Wurstbauer, U.; Gutiérrez, C.; Delongchamp, D.; Jaye, C.; Fischer, D.; Ogasawara, H.; Pettersson, L. G. M.; Reichman, D. R.; Kim, P.; Hybertsen, M. S.; Pasupathy, A. N. *Nano Letters* **2012,** 12, (8), 4025-4031.
4. Giannozzi, P.; Baroni, S.; Bonini, N.; Calandra, M.; Car, R.; Cavazzoni, C.; Ceresoli, D.; Chiarotti, G. L.; Cococcioni, M.; Dabo, I.; Corso, A. D.; Gironcoli, S. d.; Fabris, S.; Fratesi, G.; Gebauer, R.; Gerstmann, U.; Gougoussis, C.; Kokalj, A.; Lazzeri, M.; Martin-Samos, L.; Marzari, N.; Mauri, F.; Mazzarello, R.; Paolini, S.; Pasquarello, A.; Paulatto, L.; Sbraccia, C.; Scandolo, S.; Sclauzero, G.; Seitsonen, A. P.; Smogunov, A.; Umari, P.; Wentzcovitch, R. M. *Journal of Physics: Condensed Matter* **2009,** 21, (39), 395502.
5. Dean, C. R.; Young, A. F.; Meric, I.; Lee, C.; Wang, L.; Sorgenfrei, S.; Watanabe, K.; Taniguchi, T.; Kim, P.; Shepard, K. L.; Hone, J. *Nat Nanotechnol* **2010,** 5, (10), 722-726.
6. Donald, W. B.; Olga, A. S.; Judith, A. H.; Steven, J. S.; Boris, N.; Susan, B. S. *Journal of Physics: Condensed Matter* **2002,** 14, (4), 783.
7. Yazyev, O. V.; Louie, S. G. *Nat Mater* **2010,** 9, (10), 806-809.